Biasing Crystallization in Fused Silica: An Assessment of Optimal Metadynamics Parameters

Federica Lodesani,[a] Maria Cristina Menziani,[a] Shingo Urata[b] and Alfonso Pedone [a,*]

[a)] *Department of Chemical and Geological Sciences, University of Modena and Reggio Emilia, via G. Campi 103, 41125, Modena, Italia*

[b)] *Planning Department, AGC Inc., Yokohama, Kanagawa 230-0045, Japan*

*corresponding author email: alfonso.pedone@unimore.it

ABSTRACT

Metadynamics is a useful technique to study rare events such as crystallization. It has been only recently applied to study nucleation and crystallization in glass-forming liquids such as silicates but the optimal set of parameters to drive crystallization and obtaining converged Free Energy Surfaces is still unexplored.

In this work, we systematically investigated the effects of the simulation conditions to efficiently study the thermodynamics and mechanism of crystallization in highly viscous systems. As a prototype system, we used fused silica, which easily crystallizes to β-cristobalite through MetaD simulations, owing to its simple microstructure. We investigated the influence of the height, width and bias factor used to define the biasing Gaussian potential, as well as the effects of the temperature and system size on the results. Among these parameters, the bias factor and temperature seem to be most effective to sample the free energy landscape of melt to crystal transition and reach convergence more quickly. We also demonstrate that the temperature rescaling from $T > T_m$ is a reliable approach to recover free energy surfaces below T_m, provided that the temperature gap is below 600 K and the configurational space has been properly sampled. Finally, albeit a complete crystallization is hard to achieve with large simulation boxes, these can be reliably and effectively exploited to study the first stages of nucleation.

I. INTRODUCTION

Crystallization is a fundamental phenomenon that plays a key role in the production of thousands of high-tech materials used in daily life. Despite its ubiquity and a number of fundamental studies, to study quantitatively and to control precisely the amorphous to crystal transformation is still challenging.[1–5] This is mainly due to the lack of knowledge on the factors affecting the nucleation process.

Crystal nucleation is the process in which liquid, vapor, or solute particles arrange in a crystalline pattern forming an initial site for crystal growth. Whether crystallization starts from a surface, defects or in the bulk, it can be classified as heterogeneous or homogeneous nucleation. In glass-forming liquids, as silicate systems, the nucleation usually takes place from the supercooled liquid (SCL) at temperatures between the melting and the glass transition temperatures. At this temperature range, the crystal formation is thermodynamically favored and the atom mobility enables the aggregation and rearrangement of particles to form a crystalline structure. Even though unraveling the nucleation mechanism is crucial for controlling crystallization, its experimental investigation is hampered by the detection limit of the optical microscopes used to detect crystal nuclei.[6]

Molecular dynamics (MD) simulations can overcome this length scale problem but are limited to the study of events occurring at a short timescale (of the order of few ms). Therefore, MD simulations are not effective to study rare events, such as crystallization in glass-forming liquids, because crystals form and grow slowly over time. Brute-force MD simulations are applicable to study nucleation only for model Lennard-Jones liquids, compounds, and metallic alloys in which the phase transition occurs with very high nucleation rates ($>10^{35}$ nuclei$\cdot$cm^{-3}s^{-1}).[7–10] For systems exhibiting lower nucleation rates due to higher viscosity, other techniques accelerating the nucleation step have been developed and applied.

In the seeding techniques[11,12] a spherical crystalline nucleus is inserted into the supercooled liquid model. By analyzing the free energies of the systems containing different seed size, it is possible to evaluate the critical radius and the nucleation rate. The seeding technique can be extended by introducing a constraint,

which does not allow the complete dissolution of embryos to favor the crystallization. These techniques have been successfully applied to study metals and alloys,[13] ice[14] and NaCl.[15]

In the last decade, enhanced sampling techniques have been used to explore the free energy surface (FES) as a function of collective variables (CVs) appropriate to describe and follow crystallization. Metadynamics (MetaD) is one of the most used enhanced sampling techniques. It has been applied to a wide range of systems from the nucleation of molecules[16,17] and compounds[18] to metals[19] and alloys[20–22]. Recently, the method has been applied to study the crystallization of glass-forming liquids such as silica[30] and lithium disilicate system (LS_2).[23] However, to obtain converged FESs[24,25] simulations tens of microsecond-long are required . To minimize the time needed to reach convergence, optimization of the MetaD simulation set-up is fundamental. Several review articles[24] provide guidelines to appropriately choose the CVs and other parameters in MetaD simulations for organic and biological systems were CVs usually depend on few constitutive atoms, and FESs converge in nanoseconds. Contrarily, for the study of nucleation/crystallization the CVs depend on a large number of atoms. For example, one of the most used CVs to represent the degree of crystallinity is the intensity of specific peaks in the XRD patterns, which is evaluated from the positions of hundreds of atoms in the simulation box.[25] Therefore, in the study of crystallization of highly viscous systems the MetaD simulation set-up used for molecular systems cannot be applied, and further investigation is necessary for effective MetaD simulations.

A systematic study of the effect of MetaD parameters, temperature, and system dimension is carried out in this work to effectively obtain converged Free-Energy Surfaces in glass-forming liquids. We selected silica as a prototypical material of silicates because β-cristobalite can crystalize relatively easily through MetaD simulations owing to its simple microstructure.

II. METHOD

A. *Standard and Well-tempered Metadynamics*

In standard MetaD simulations,[26] the free energy landscape along a set of CVs (**s**) is evaluated by including a history-dependent bias $V(\boldsymbol{s},t)$ to the potential, which is composed of Gaussian functions accumulated along the simulation:

$$V(\boldsymbol{s},t) = \sum_{t\prime<t} \omega \, exp\left[-\sum_{\alpha=1}^{N_{CV}} \frac{\left(\boldsymbol{s}_\alpha - \boldsymbol{s}_\alpha(t')\right)^2}{2{\sigma_\alpha}^2}\right] \quad , \quad t' = k\tau \qquad (1)$$

where ω is the height of the Gaussian centered in the visited point of the CV space, $\boldsymbol{s}(t')$, at each MetaD step, t', with a width σ. Each MetaD step is k-times of the Gaussian deposition time, τ.

In Well-Tempered Metadynamics (WTMetaD),[27] the height of the Gaussian added at each timestep is scaled down by a factor, which depends on the bias already accumulated and the bias factor, γ:

$$V(\boldsymbol{s},t) = \sum_{t\prime<t} \omega \, exp\left[\frac{-1}{\gamma-1}\beta V(\boldsymbol{s}(t'),t')\right] exp\left[-\sum_{\alpha=1}^{N_{CV}} \frac{\left(\boldsymbol{s}_\alpha - \boldsymbol{s}_\alpha(t')\right)^2}{2{\sigma_\alpha}^2}\right] \quad , \quad t' = k\tau \qquad (2)$$

where $\beta=(k_BT)^{-1}$ is the inverse temperature, the factor $(\gamma-1)\beta^{-1}$ is sometime referred to as $k_B\Delta T$. The bias factor is an indicator of how fast the height of Gaussians will decrease during the simulation, and it determines the effective temperature along the biasing CV, which is $(T+\Delta T)=\gamma T$. In the WTMetaD, the bias potential tends to increase with the same intensity at each point in the CV space, which results faster converging than non-tempered MetaD by avoiding the exploration of very high-energy regions. From the accumulated bias potential, the free energy surface of the investigated transition can be estimated as:

$$F(\boldsymbol{s}) = \frac{-\gamma}{\gamma-1} V(\boldsymbol{s}) \quad . \qquad (3)$$

The procedure to determine the bias potential is crucial for accurately reconstructing the FES, and selection of the parameters is sensitive to convergence time of the simulation. Height, ω, width, σ, and bias factor, γ, are the WTMetaD parameters, which define the shape of the Gaussians added during the simulation. The deposition time, τ, is another important parameter, but, in this work, we set it to be a constant value.

Bussi and Branduardi[24] provided the following hints on how to choose the WTMetaD parameters: i) The height is suggested to be a fraction of thermal energy (k_BT), to avoid abrupt changes to the total potential; ii) the width should be a fraction of the standard deviation of the CV-values obtained from an unbiased MD simulation of the system. iii) the bias factor is suggested to be the energy corresponding to the barrier height associated to the transformation. These are reasonable suggestions when one-component systems or particles possessing a moderate atomic mobility transform with relatively low and known activation energy. However, for glass forming liquids, it is difficult to make a fast estimation of the correct parameters.

To check the effect of each WTMetaD parameter, we used the convergence time and the transition (re-crossing) frequency as indicators of the performance, in addition to the accuracy of the re-constructed FES. In the case of the unbiased MD simulations, the FES is computed by unbiased ensemble averages $\langle O(\boldsymbol{R})\rangle$, where $\boldsymbol{R}$ represents the atomic configurations of the system. Contrarily, the FES is calculated using the reweighting procedure,[28] which recovers the FES along the CVs biased in the WTMetaD simulations. Each configuration of the trajectory is weighted according to the bias deposited. Then, the unbiased Boltzmann probability distribution $P_0(\boldsymbol{R})$ is estimated by reweighting the biased distribution $P(\boldsymbol{R},t)$:

$$P_0(\boldsymbol{R}) = P(\boldsymbol{R},t)w_V(\boldsymbol{R}), \qquad w_V(\boldsymbol{R}) = e^{\beta\left(V(\boldsymbol{s}(\boldsymbol{R}),t)-c(t)\right)}\ , \tag{4}$$

where the exponential part is the weight for each configuration, and $c(t)$ is a time-dependent function of the offset energy, which estimates the work done by the bias. An increase of the offset energy indicates that the FES approaches to an asymptotic approximation. In fact, once the applied bias becomes quasi-stationary, the adiabatic limit is reached, and, thus, the FES is recovered. The offset energy, c(t), can be evaluated using different formulas,[28,29] in this work we used the one suggested in the review of Valsson et al.[30]:

$$c(t) = \frac{1}{\beta} log \frac{\int d\boldsymbol{s} exp\left[\frac{\gamma}{\gamma - 1}\beta V(\boldsymbol{s}, t)\right]}{\int d\boldsymbol{s} exp\left[\frac{1}{\gamma - 1}\beta V(\boldsymbol{s}, t)\right]} \quad . \qquad (5)$$

The average of a general observable can be estimated from the trajectory as the unbiased ensemble $\langle O(\boldsymbol{R})\rangle_0$:

$$\langle O(\boldsymbol{R})\rangle_0 = \left\langle O_b(\boldsymbol{R}) e^{\beta\left(V(\boldsymbol{s}(\boldsymbol{R}),t) - c(t)\right)}\right\rangle \quad . \qquad (6)$$

It is thus possible to extract the probability distribution for each CV, $\boldsymbol{s}'$, using eq. (4) and (6). Then, according to $O(\boldsymbol{R}) = \delta[\boldsymbol{s}' - \boldsymbol{s}'(\boldsymbol{R})]$, we obtain:

$$P(\boldsymbol{s}') = \int d\boldsymbol{R}\delta[\boldsymbol{s}' - \boldsymbol{s}'(\boldsymbol{R})]P_0(\boldsymbol{R}) = \int d\boldsymbol{R}\delta[\boldsymbol{s}' - \boldsymbol{s}'(\boldsymbol{R})]P(\boldsymbol{R}, t)e^{\beta\left(V(\boldsymbol{s}(\boldsymbol{R}),t) - c(t)\right)} \quad , \qquad (7)$$

from which the FES can be easily calculated:

$$F(\boldsymbol{s}') = -\frac{1}{\beta} log P(\boldsymbol{s}') \quad . \qquad (8)$$

The error of the FES was evaluated by comparing FES computed using several blocks of configurations extracted along the trajectory.[31] The simulations was judged to be converged when the error remains constant with an increase of the block sizes.

B. *Rescaling procedure*

In our recent work,[23] which studied crystallization of lithium disilicate using WTMetaD, very slow dynamics even at melting temperature prohibits the observation of the number of crystallization events necessary to reach converged FESs. For this reason, a temperature rescaling method was applied to estimate the free-energy landscape at the melting temperature. In this method, the probability distribution, $P(\boldsymbol{R},t)$, calculated by a WTMetaD simulation at a higher temperature is reweighted to estimate the probability distribution at a lower temperature, $P'(\boldsymbol{R})$. The idea is similar to the reweighting calculation using eq. (4). The reweighting factors, w, for a canonical ensemble (NVT) and an isothermal-isobaric ensemble (NPT) are respectively defined as:

$$w_{NVT}(\boldsymbol{R}) = e^{(\beta-\beta\prime)U(\boldsymbol{R})} \text{ or } w_{NPT}(\boldsymbol{R},V) = e^{(\beta-\beta\prime)(U(\boldsymbol{R})+pV)} \quad (9)$$

where $U(\boldsymbol{R})$ is the internal energy of each configuration, $U(\boldsymbol{R})+pV$ is the enthalpy, and β and β' are the target and original inverse temperatures.

C. *Collective variable*

As a CV, an intensity of a specific X-ray diffraction (XRD) peak calculated using the Debye scattering formula was considered:[32]

$$I(Q) = \frac{1}{N}\sum_{j=1}^{N}\sum_{i=1}^{N} f_i(Q) f_j(Q) \frac{sin(Q \cdot r_{ij})}{Q \cdot r_{ij}} W(r_{ij}) \quad . \quad (10)$$

where $f_i(Q)$ and $f_j(Q)$ are the atomic scattering form factors, Q is the scattering vector modulus, and r_{ij} is the distance between atoms i and j. $W(r_{ij})$ is the Lorch function used to overcome the artifacts due to the finite simulation box, and it is calculated as:

$$W(r_{ij}) = \frac{sin(\pi\, r_{ij}/R_c)}{\pi\, r_{ij}/R_c} \quad . \quad (11)$$

where R_c is the upper limit for r_{ij}.

Contrary to the previous work by Niu et al.,[33] where $I(Q)$ was evaluated using all atoms, in this work, only silicon atoms were considered to reduce the computational cost. The WTMetaD simulation accuracy is not sacrificed because oxygen positions are related to silicon positions when promoting crystallization. By comparing the XRD patterns of crystalline and amorphous structures, the Q value exhibiting the biggest difference in the intensity peak was selected as and effective CV. Note that Q value is converted to a scattering angle 2θ *as*:

$$Q = \frac{4\pi}{\lambda} sin\theta \quad , \quad (12)$$

where λ is the wavelength of the radiation (in this work 1.5406 Å). According to Figure 1, which shows the XRD patterns obtained from 2 ns of unbiased MD simulations of β-cristobalite and silica melt using 192 atoms at 2400K, the peak intensity at $2\theta = 22°$ is found to be suitable for distinguishing the crystalline and amorphous structures. It is worth noting that other CVs representing local structures have been successfully used to drive crystallization of water and ionic systems;[34,35] however, local structural parameters are ineffective for silicate systems because they cannot distinguish chains, rings, and layered structures of silicates.

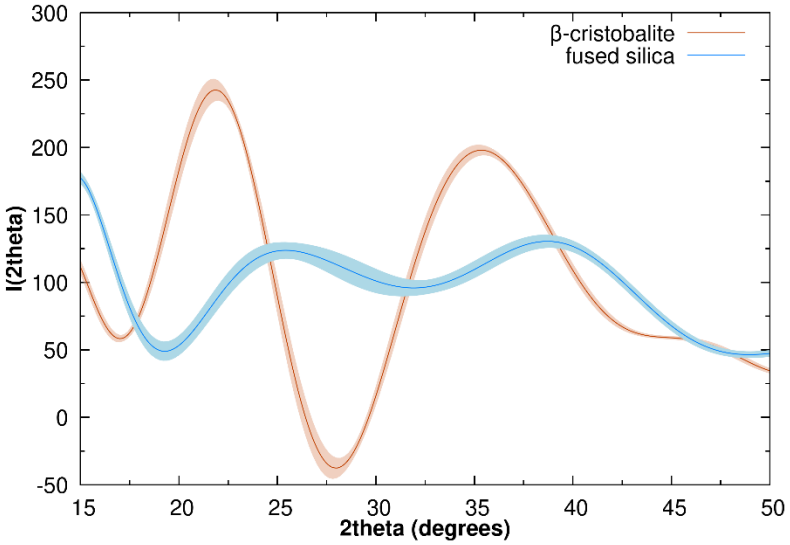

FIG. 1. XRD spectra of the crystalline (β-cristobalite) and silica melt by considering only Si atoms. The XRD spectra are averaged along the 2 ns of MD trajectory, and the standard deviation is represented with a shaded region.

III. **COMPUTATIONAL DETAILS**

In this work, we investigated the fused silica - β-cristobalite transformation. All initial configurations were obtained by replicating the cristobalite crystalline unit cell,[36] which contains 24 atoms in a cubic lattice with size of 7.12 Å, to a larger model. We employed the interatomic potential developed by Pedone

et al.[37] for pair-wise short-range interactions, while long-range Coulomb interactions were described by using Wolf summation method.[38] The large-scale atomic/molecular massively parallel simulator (LAMMPS)[39] software patched with a plugin for molecular dynamic (PLUMED)[40] was used for all MD and WTMetaD simulations. In all simulations, the Nosé-Hoover thermostat[41] and barostat were employed for performing NVT or NpT simulations at 1 bar. The relaxation times for controlling temperature and pressure were 0.1 ps and 10 ps, respectively. All WTMetaD simulations were performed using NPT ensemble. The equation of motion was integrated using the Verlet algorithm[42] with a timestep of 2 fs.

The WTMetaD parameters setting tested are reported in Table I. Each parameter was varied between a couple of values: ω-values are 20 and 60 kJ/mol, σ-values are 2 and 8 CV units, while γ-values tested are 20, 50 and 150.

TABLE I: List of experimental conditions tested to examine the effect of WTMetaD parameters

n° experiment	**ω (kJ/mol)**	**γ**	**σ (CV units)**
1	20	50	2
2	20	50	8
3	20	150	2
4	60	50	2
5	60	50	8
6	60	150	2
7	60	20	2

All simulations in this test set were performed with a unit cell containing 192 atoms (2x2x2) at T=2700 K. The effect of the temperature was studied at 3200 K and 2700 K. The simulation size effect was studied by performing some simulations with unit cells containing 648 (3x3x3) and 1536 (4x4x4) atoms.

IV. **RESULTS**

To rigorously investigate the effects of the parameters listed in Table I, WTMetaD simulations were performed for 10 μs at 2700 K. In the following, we will show in the main text only the comparisons among selected simulations to highlight significant results, whereas all the remaining results are reported in the Supplementary Material (ESI). First, we will discuss the procedure used to analyze a single simulation, because it will clarify all results that will follow.

A. *How to analyze a simulation*

The time evolution of the CV used to bias the simulation gives information about the diffusivity of the system between the crystal and amorphous states. In Figure 2, the simulation n° 4 (ω=60, γ=50, σ=2) is chosen as an example.

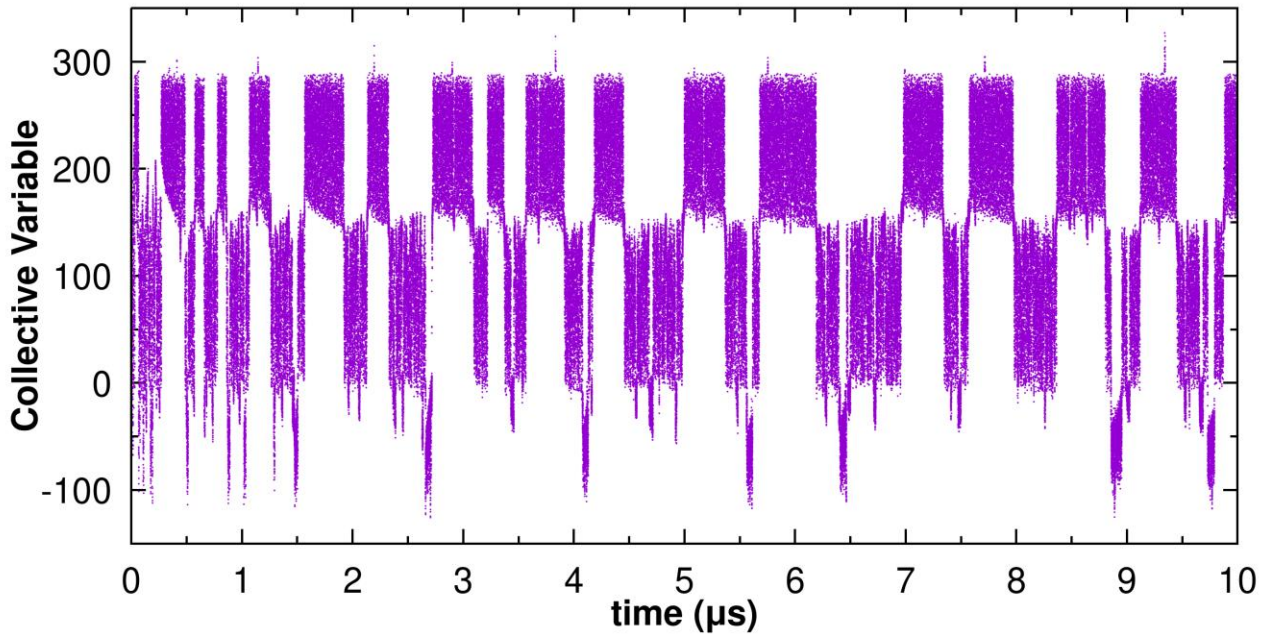

FIG. 2. Time evolution of the CV in WTMetaD simulation n° 4 at 2700 K

The transitions are frequently observed along the simulation. The crystalline phase is located at high value of the CV, between 150 and 300, while the melt phase is in the region between 0 and 150. The other CV-values explored are associated to high-energy structures, which are not important to understand the mechanism of the crystallization.

The trend of the offset energy, c(t), shown in Figure 3 demonstrates how the applied bias varies. The re-crossing frequency, which is the number of transitions between solid and liquid per unit time during the WTMetaD, can be an indicator of the diffusivity.[25] Assuming the adiabatic regime appears from 4 μs, the re-crossing frequency of simulation n° 4 is on average 2.5 re-crossings per micro-second. Note that, as expected from the theory of MetaD, the c(t) rapidly increases in the initial stage followed by a slower increasing in the quasi-stationary bias region that indicates that the asymptotic regime in which WTMetaD is valid has been reached. Albeit the achievement of asymptotic regime has been used as indication of converged simulations in previous works, we will show in the following that this is not always the case.

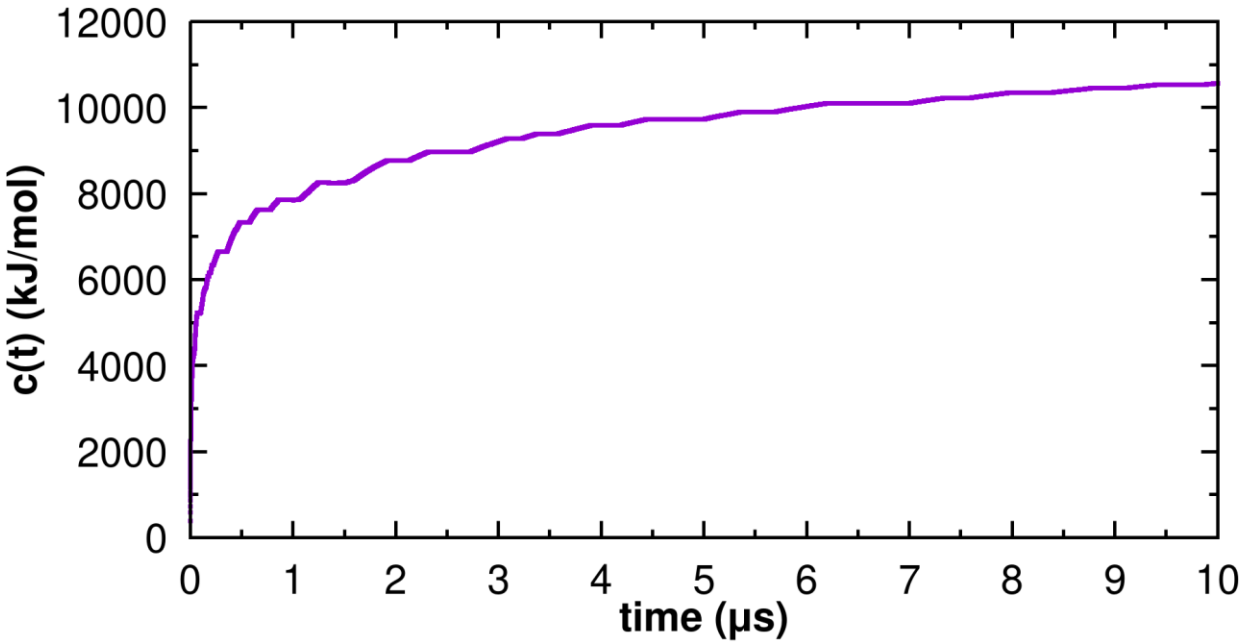

FIG. 3. The offset energy c(t) as a function of simulation time for simulation n° 4.

The FES can be evaluated once the adiabatic regime is reached using two approaches. The first approach accumulates the bias and estimates the FES using the eq. (3). However, if the additional bias is not completely stationary (a criterion satisfied only over infinite time) the calculated FES keeps changing. This behavior is observed in Figure 4 (a). In fact, the variation of the FES curve tends to decrease as the simulation proceeds, but it does not converge. Interestingly, the estimated FES fluctuates around the correct FES beyond the diffusive regime. Therefore, a cumulative average potential and an average of FES can be evaluated. This procedure is usually applied in the non-tempered MetaD simulations,[43] because for the WTMetaD the average FES converges by construction as the applied potential decreases with time.[44] It is still a useful procedure, not for the estimation of the error in the free energy calculation, but to understand the convergence. The averaged FES is reported in Figure 4 (b). We started to accumulate the potential after the two free-energy wells are filled. Accordingly, the FES curve converges relatively quickly at around 5-6 μs. The last approach is the reweighting procedure described by eqs. (4) and (8). The error of the FES was estimated using the block analysis.[31]

The following step is to understand which part of the simulation has to be accounted for accumulating the probability distribution. According to Figure 3 and Figure 4(a), it is clear that the quasi-static regime has not been reached before 4-5 μs, therefore, we should not take the earlier configurations into account. We selected different starting point to see how the calculated FES changes and progresses over time. Figure 4 (c) shows an overview of some reweighted FESs. In this figure, color ranges are associated to five different starting points, as indicated in the color bar on the right side of the plot. Even though the reweighted FESs obtained from 0 and 2 μs are not meaningful from physical viewpoint, they are also compared to understand what happens in the non-adiabatic regime to estimate the FES.

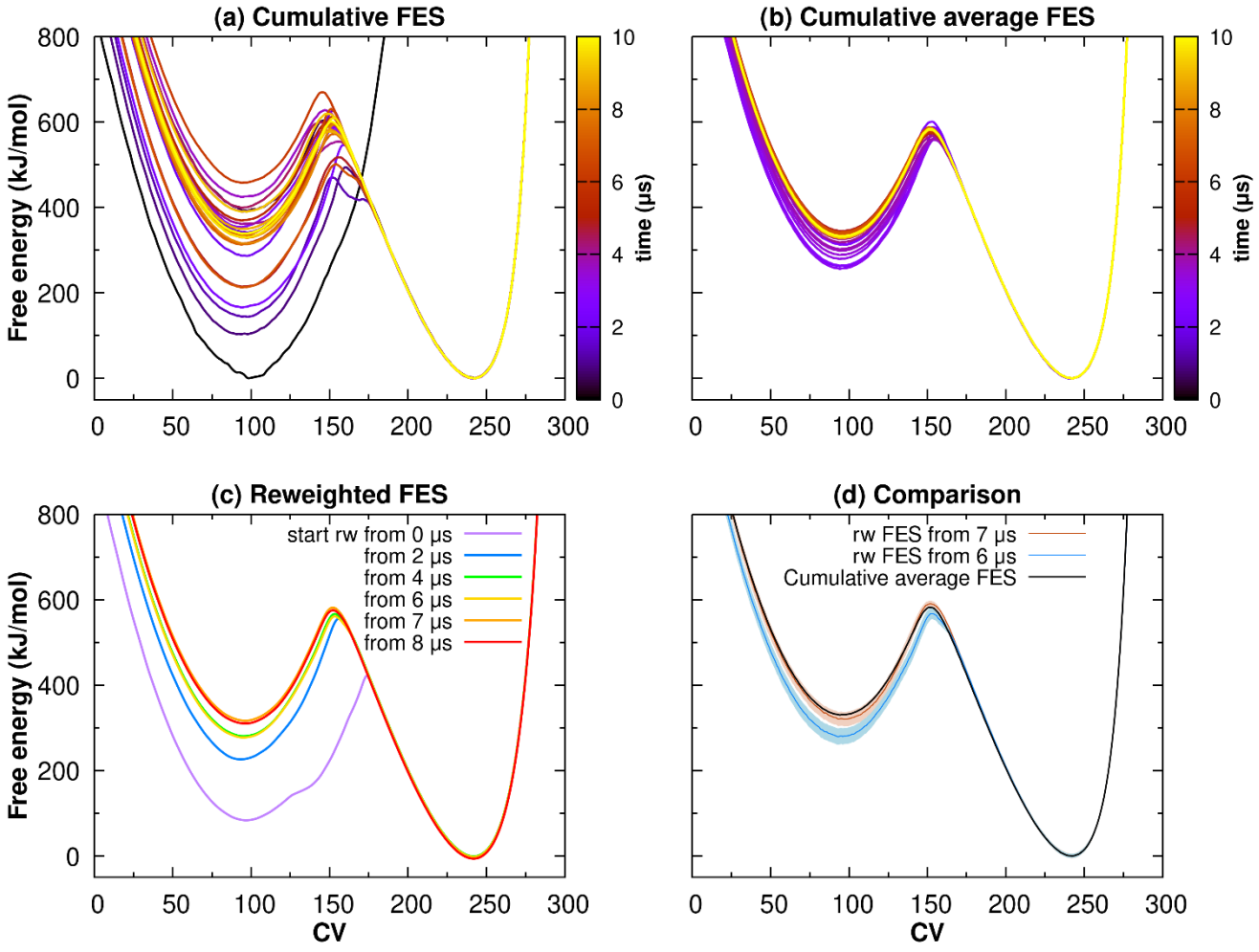

FIG. 4. Different methods to calculate FES of simulation n° 4. (a) Cumulative bias is evaluated and using eq. (3) free energy is calculated at each time. (b) After a suitable initial time, the average of the cumulative bias at different time is calculated. (c) FESs were evaluated using reweighting procedure applied starting

from different simulation time. (d) Comparisons of final FESs obtained with averaging and reweighting methods; the second ones report the error calculated with the block analysis

The choice of the starting time is crucial to calculate the correct FES, because, in fact, the reweighted FES keeps changing until 7 μs. After 7 μs, the longer simulation do not vary the FES shape. Figure 4 (d) compares the FESs obtained by the cumulative averaging and reweighting procedures. The latter FES is shown with standard deviations. The FES reweighted form 7 μs agrees well with cumulative averaged one. The sufficiently small error calculated from the block analysis proves the convergence. As shown in Figure 5, the error was evaluated with different block sizes. The plateau independent from the block dimension after approximately one hundred thousand blocks gives the average error of the FES.

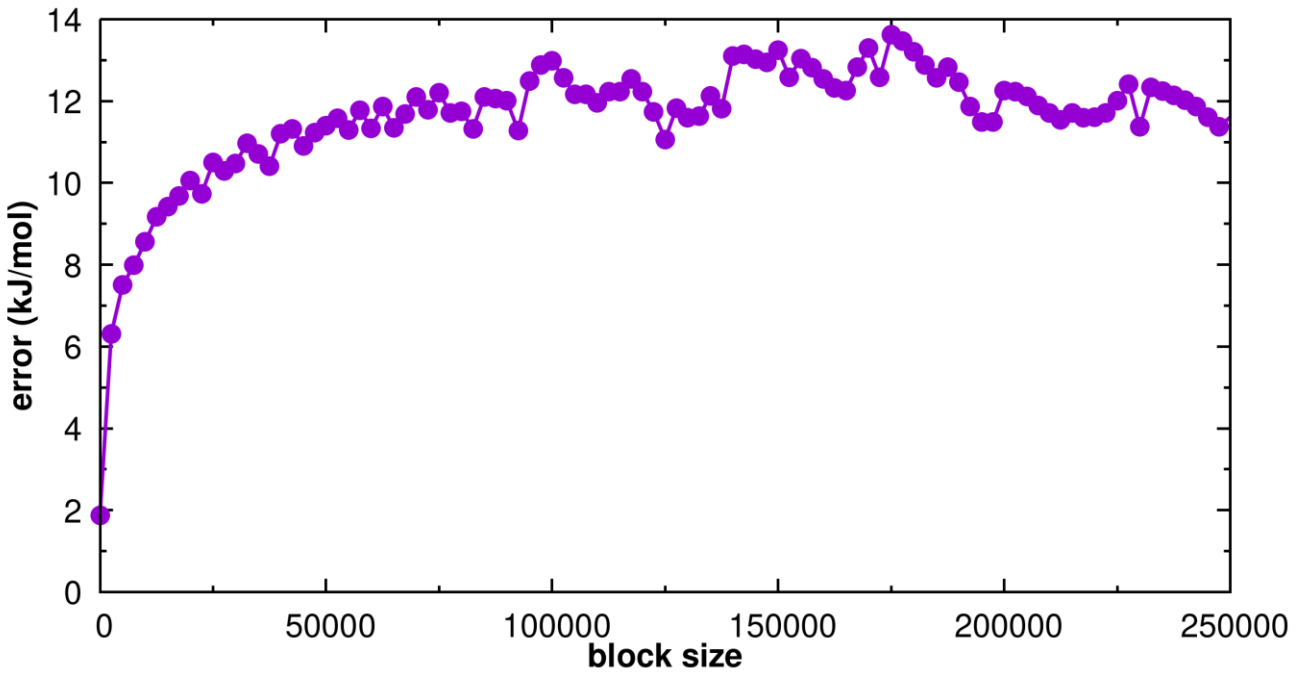

FIG. 5. The error of FES obtained from block analysis on probability distribution histogram accumulated starting from 7 μs to 10 μs.

Tiwary and Parrinello[28] defined the time-independent estimator as eq. (13) to confirm the free energy convergence in a given small region of the CV space:

$$\beta F(s) = \frac{-\gamma V(\boldsymbol{s},t)}{k_B \Delta T} + log \int d\boldsymbol{s} e^{\gamma V(\boldsymbol{s},t)/k_B \Delta T} \quad . \qquad (13)$$

From eq. (13), the difference between the free energies in two small regions s_1 and s_2 can be obtained:

$$\Delta F_{s_1,s_2} = \frac{-\gamma}{\gamma - 1} \Delta V_{s_1,s_2} \quad , \qquad (14)$$

$\Delta F_{s1,s2}$ is equivalent to the direct difference in free energy obtained by the accumulated bias within the two states. Because $\Delta F_{s1,s2}$ can be calculated during the WTMetaD simulations, it is also an indicator of the FES convergence, at least, at the two small regions s_1 and s_2. We call this parameter *direct* ΔF.

The ΔF between the basins can be also calculated from the probability distributions obtained during the reweighting procedure.

The relative reweighted free energy difference between state A and B can be correctly determined from F(**s**) by integrating the probabilities of the two states (according to eq. (8)).

$$\Delta F_{A,B} = -\frac{1}{\beta} log \frac{P_A}{P_B} = -\frac{1}{\beta} log \frac{\int d\boldsymbol{s}\, e^{-\beta F(s)}}{\int d\boldsymbol{s}\, e^{-\beta F(\boldsymbol{s})}} \quad . \qquad (15)$$

By assuming that states A and B are two wells, the difference in height between the two free energy minima is a possible approximation of ΔF,[45] if the shapes of the two basins are similar. We call this parameter *reweighted* ΔF to use as another estimator of FES convergence despite the lower accuracy. Both the direct and reweighted ΔF should converge to the same value if they are calculated in the same region, as the total free energy surfaces agree each other. If the reweighted ΔF does not agree with the direct ΔF, the probability distribution might be corrected from the non-adiabatic region. It is important to ensure that the accumulation is started from the quasi-stationary regime to collect meaningful probability distributions. The direct and reweighted ΔF are less accurate but faster and more practical indexes than the complete FES. In Figure 6, these estimators are compared.

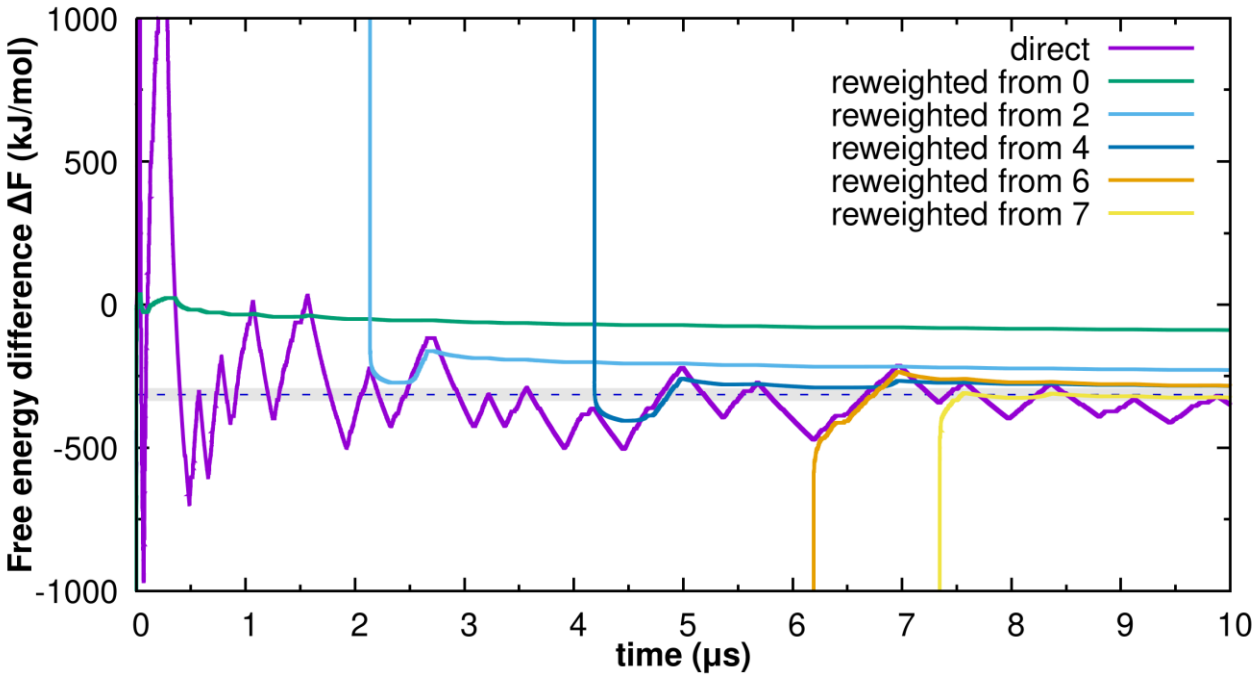

FIG. 6. ΔF between the minima of the two states obtained directly from the acting bias and from the reweighting procedure started at different starting time. The dotted line indicates the final average value with a blue stripe representing 1 k_BT width.

The reweighted ΔF converges faster than the direct ΔF; however, it converges to the correct value only when it is calculated from the adiabatic regime. The block analysis can be used to judge whether the sampling is sufficient or not.

B. *Effect of MetaD parameters (ω, σ, γ)*

In this section, the comparisons among several selected simulations are shown to highlight the importance of the parameter choice. In particular, we discuss the best parameter set for obtaining a faster and more accurate convergence.

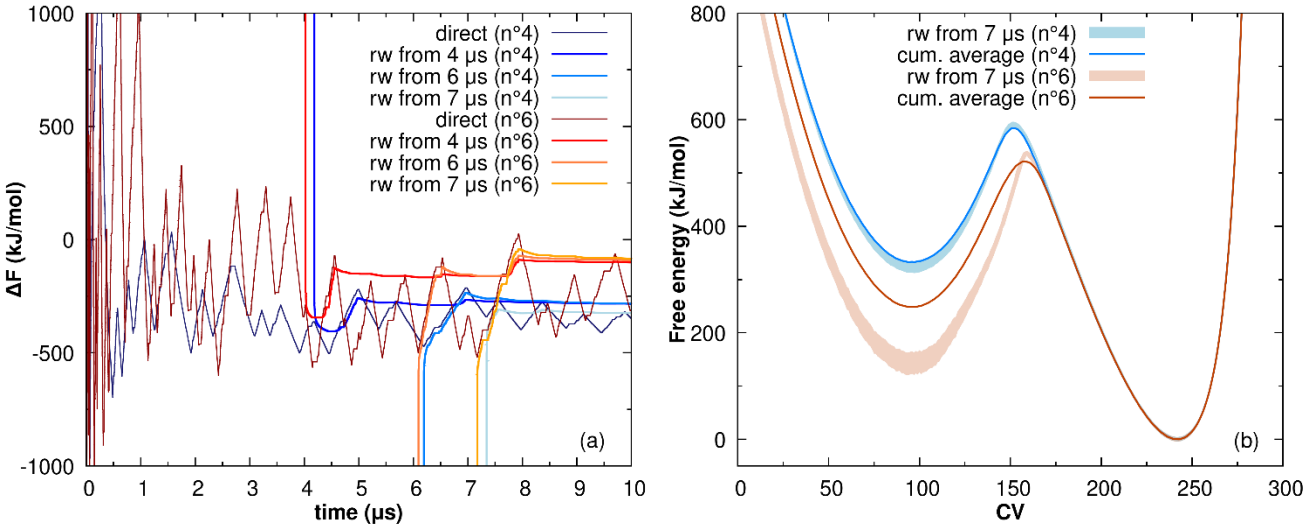

FIG. 7. (a) Direct and reweighted ΔF calculated for simulation n° 4 (ω=60, γ=50, σ=2) and n° 6 (ω=60, γ=150, σ=2), which differ in γ value. (b) Comparison between FESs obtained from the two simulations using reweighting and cumulative average procedures.

Figure 7 reports the results of simulations n° 4 (ω=60, γ=50, σ=2) and n° 6 (ω=60, γ=150, σ=2), which differ only in the bias factor value. The direct and reweighted ΔF are compared to see the effect of the bias factor, γ, in Figure 7 (a). The direct ΔF of n° 6 exhibits a greater fluctuation, meaning considerable variations of the cumulative FESs over time and a higher re-crossing frequency. Contrarily, as shown in Figure 2, simulation n° 4 (ω=60, γ=50, σ=2) exhibits smaller fluctuations and re-crossing frequency. Figure 7 (b) shows that in simulation n° 6 (ω=60, γ=150, σ=2) the reweighted FESs calculated from different starting times do not converge with the average value of the cumulative FES, implying that the adiabatic region is not reached. The time evolution of the CV for simulation n° 6 (shown in Figure S1 of the ESI) reveals that the bias factor, γ=150, is too high and pushes the system to explore high-energy CV regions, which are not important to understand melt-crystal transition. The exploration of these high energy regions can be controlled constraining the dynamics in a certain region of the CV.[46] However in this case we have not observed an improvement in the convergence speed, since the time spent in the high-energy region is not significant.

The FES does not converge neither in simulation n°3, which also has a high value of γ (results in Figure S2 of ESI). On the other hand, simulation n° 7 (ω=60, γ=20, σ=2), which has a low γ-value, presents small fluctuations but too low diffusivity (Figure 8 (a)) to obtain the converged FES in reasonable simulation time. Indeed, the block analysis reported in Figure 8 (b) confirms that the simulation n° 7 does not reach convergence until 10 μs.

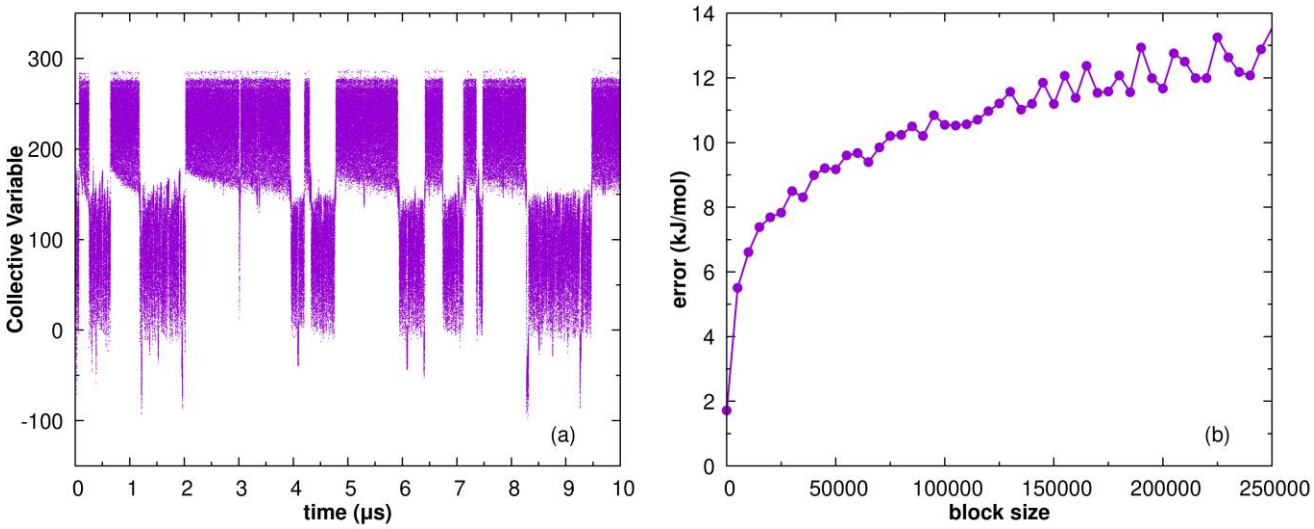

FIG. 8. (left) Time evolution of the CV in WTMetaD simulation n° 7 (ω=60, γ=20, σ=2) at 2700K, (right) estimation of the error using the block analysis on the probability distribution.

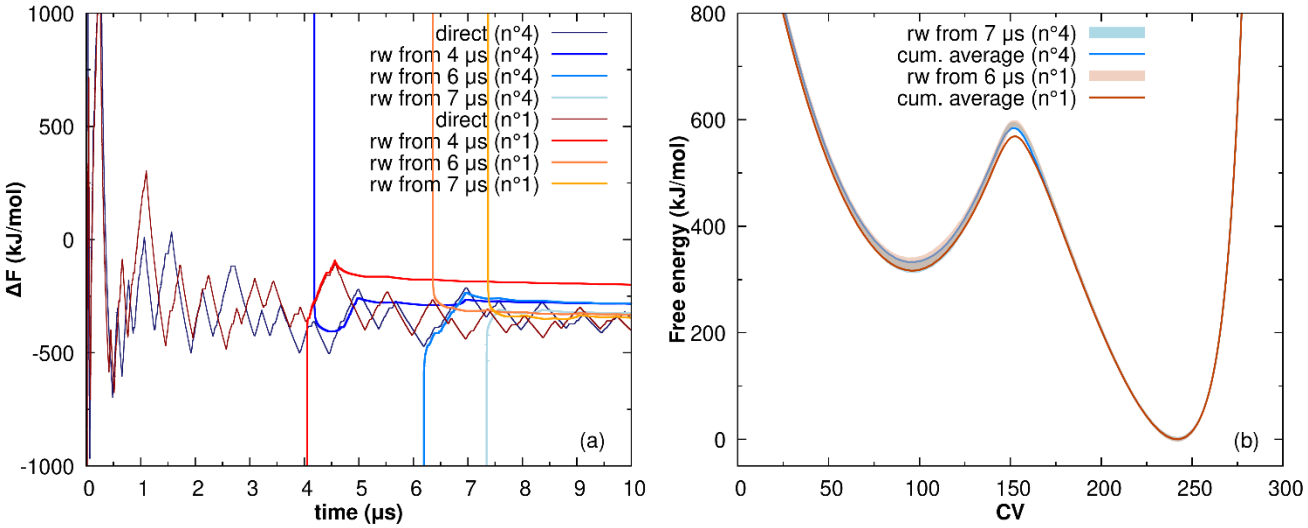

FIG. 9. (a) Direct and reweighted ΔF calculated for simulation n° 4 (ω=60, γ=50, σ=2) and n° 1 (ω=20, γ=50, σ=2), which differ in ω value. (b) Comparison between FESs obtained from the two simulations using reweighting and cumulative average procedures.

Figure 9 compares simulations differing in the height, ω, which was 20 kJ/mol for simulation n° 1 (ω=20, γ=50, σ=2) and 60 kJ/mol for n° 4 (ω=60, γ=50, σ=2). Both the FESs and ΔF almost perfectly match. The re-crossing frequency is also not affected by the value of ω.

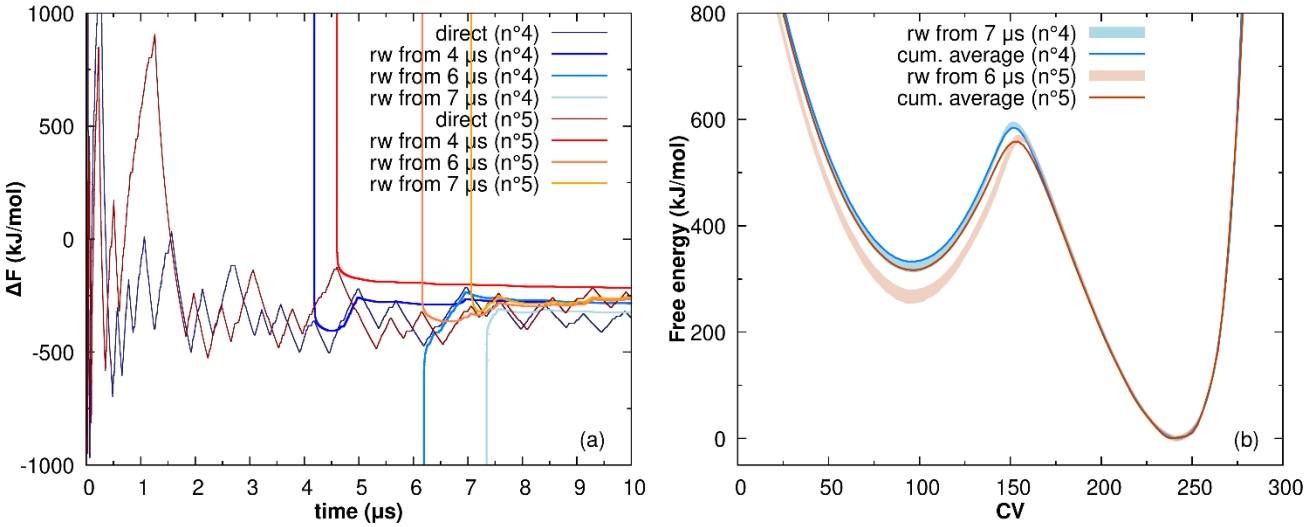

FIG. 10. (a) Direct and reweighted ΔF calculated for simulation n° 4 (ω=60, γ=50, σ=2) and n° 5 (ω=60, γ=50, σ=8), which differ in σ value. (b) Comparison between FESs obtained from the two simulations using reweighting and cumulative average procedures.

Figure 10 compares simulations n° 4 and n° 5 differing in the width of the Gaussian: σ=2 and σ=8, respectively. The width must be chosen carefully, because it spreads the bias in the region near the explored CV. It accelerates filling the wells in a more efficient way, resulting in a faster decrease of the height of the Gaussians. Contrarily, the phase space associated to each state has to be sufficiently larger than the width of Gaussians, otherwise the bias affects outside of the interested regions. Usually, the possible choice of σ is estimated by the fluctuation of the CV using unbiased MD simulations. In our case, the standard deviations of the CV were approximately 7 CV units and 9 CV units in the crystalline and the melt phases, respectively (see Figure 1). Indeed, simulation n° 4 whose σ value is a fraction of the standard deviations converged, while simulation n° 5 did not probably due to the larger bias. The similar behaviors were observed for the other simulations when the Gaussian width is too large.

Only a few simulations, n° 1 (ω=20, γ=50, σ=2) and n° 4 (ω=60, γ=50, σ=2), converged at 2700K within 10 µs. The agreement between the cumulative average and the reweighted FESs is obtained only in those two simulations, but also simulation n° 2 (ω=20, γ=50, σ=8), n° 5 (ω=60, γ=50, σ=8) and n° 7 (ω=60,

γ=20, σ=2) obtained similar curves (see Figure S3-S4 in the ESI). These results indicate predominant effect of the bias factor. Increasing the bias factor leads to higher transition rates and affects the exploration of the phase space. An appropriate choice of the bias factor may allow overcoming very high barrier to see unlikely processes, reaching high-energy configurations. On the other hand, exploring such high-energy regions increases the simulation time to reach convergence in the stable regions of interest. In our specific case, γ=50 is the best choice. σ=2 is a good choice since it allows to reach convergence faster, while height, ω, is less influential even though simulation n° 1 (ω=20, γ=50, σ=2) reached convergence slightly earlier than n° 4 (ω=60, γ=50, σ=2), as shown in Figure 9 (a).

C. *Effect of the temperature*

To investigate the effect of the temperature, all experiments in Table I were examined at 3200 K as well, but for the sake of brevity we focus only on the results of experiment n° 4 (ω=60, γ=50, σ=2). Figure 11 shows the time evolution of the biasing CV (peak at 2θ=22°) at the two temperatures. The frequency shuttling between the two states is much higher at 3200 K due to the higher diffusivity and atomic mobility. This enables a more efficient sampling of the configurational space and thus to obtain the crystallization pathway. Consequently, the simulations at higher temperatures converge easier. Figure 12 shows the fluctuations of the direct and reweighted ΔF for the two temperatures.

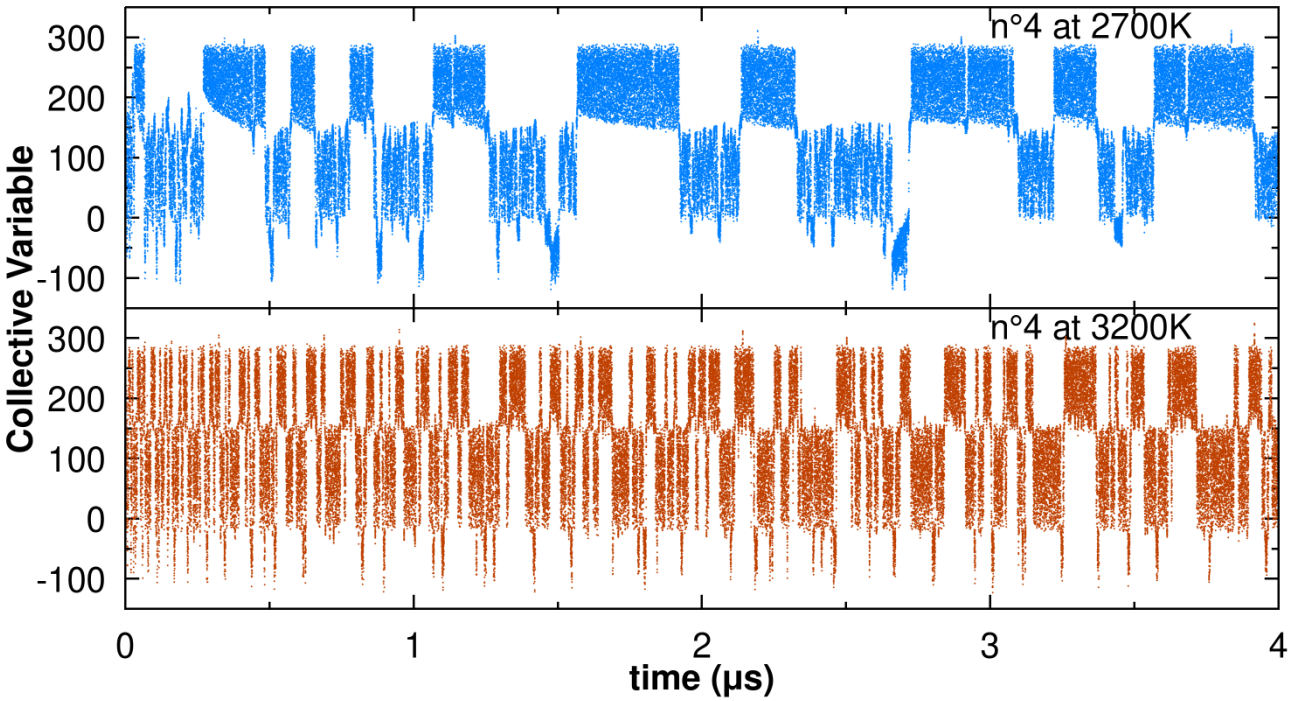

FIG. 11. Time evolution of the CV during 4 μs of WTMetaD simulation of experiment n° 4 (ω=60, γ=50, σ=2) at 2700 K and 3200 K.

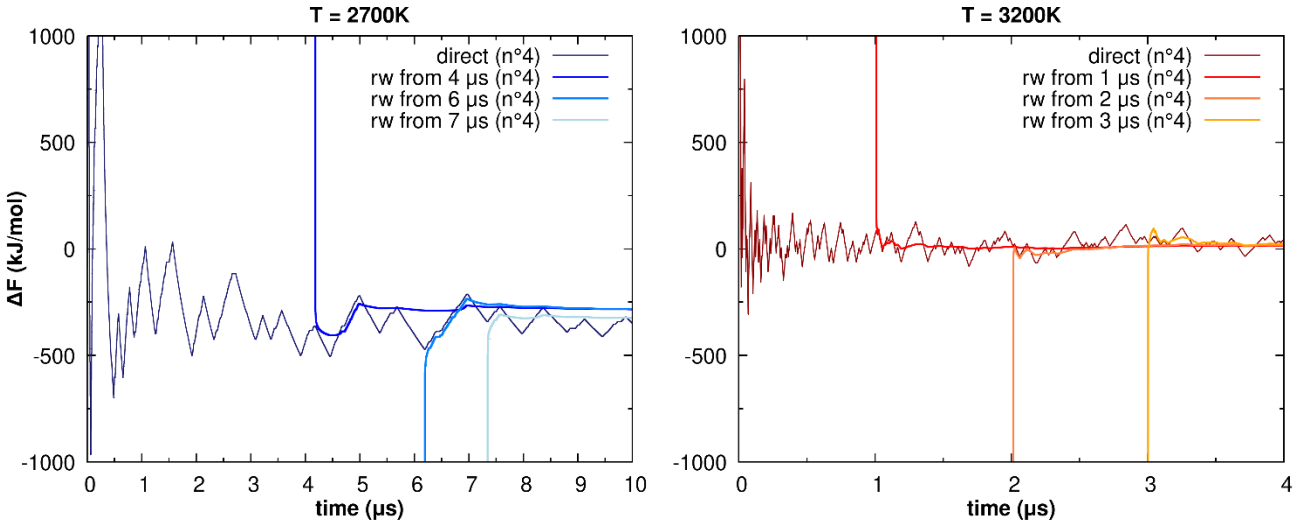

FIG. 12. Comparison between direct and reweighted ΔF for simulation n° 4 (ω=60, γ=50, σ=2) at 2700 K (left) and 3200 K (right).

At 3200 K, the reweighted and direct ΔF agree well because both converge to the average value, whereas at 2700 K the simulations do not converge. Moreover, lower fluctuations and lower error (6.5 kJ/mol) of the direct ΔF were observed at 3200 K with respect to those at 2700 K, at which the error was 12 kJ/mol, as shown in Figure 5. All simulation conditions in Table I at 3200 K converge towards the same FES faster than at 2700 K regardless of the parameter sets (reported in the ESI in Figure S5). Therefore, temperature seems to be the most important factor to reach accurate FES using WTMetaD, especially for highly viscous systems as silicate melts.

To obtain converged FES at the melting temperature or lower, several tens of microseconds of simulations would be required for silicates. In such cases, one possible alternative method is reweighting a high-temperature distribution probability to a lower temperature one, as described in the section II B.

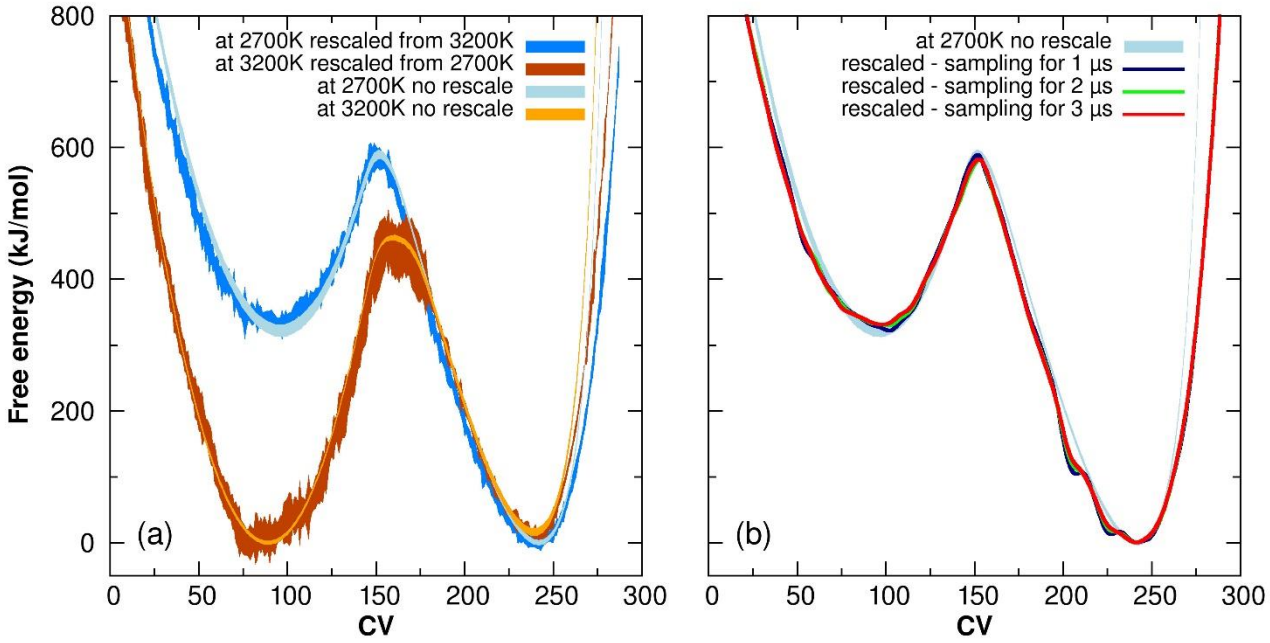

FIG. 13. (a) Comparison between FESs calculated directly from the simulations n°4 (ω=60, γ=50, σ=2) at 3200K (starting from 1 μs) and 2700K (starting from 7 μs) and using the rescaling procedure from one temperature to the other. (b) The reweighted FES obtained at 2700K is compared with rescaled curve from 3200K using different sampling intervals; the curve becomes smoother as the sampling increases.

The reliability of the temperature reweighting method is verified by evaluating the FES associated with the crystallization of β-cristobalite from silica melt, as shown in Figure 13. The rescaling procedure was applied at both temperatures using 3 μs of simulations, from 1 to 4 μs at 3200 K and from 7 to 10 μs at 2700 K. These results show that the temperature reweighted FES (from 3200 K to 2700 K) reproduces well (within the simulation error) the FES directly obtained from the WTMetaD simulation at 2700 K, even though with a larger error. The same is true if we convert the FES at 2700 K to 3200 K, confirming the reliability of this approach.

The roughness and the error of the rescaled FES from 2700 K to 3200 K (red curve) in Figure 13 (a) is higher than that of the rescaled FES from 3200 K to 2700 K (blue curve) because of the poorer sampling performed at lower temperature, 2700K, and for the large fluctuation of the associated weights. Longer simulation to better sampling the phase space makes the curve smoother, as observed in Figure 13 (b). Because it is expected that the roughness of the rescaled FES increase with an increase of the temperature gap, which should not exceed 500-600 K to avoid undesired artifacts. Parallel tempering Metadynamics[47] simulations is an alternative technique to test in future investigations to reduce the final error on the FES.

D. *Size effect*

In real materials, homogeneous nucleation occurs stochastically in the bulk of the melt, leading to the formation of several critical nuclei that grow until they impinge each other for forming polycrystalline materials or glass-ceramics. The observation of such whole process in computer experiments would require extremely large simulation models with at least millions of atoms, which are too expensive for MetaD simulations. Because much of the scientific interest is addressed to the formation of the critical nuclei, such as CNT, it is worth investigating the initial process of the nucleation. In principle, crystallization should be investigated using simulation boxes much larger than the critical nuclei, but this is not always possible since the critical dimensions strongly depend on the materials and in silicates can

range from a few angstroms to nanometers.[48] Nevertheless, it is thus important to investigate the effect of the system dimensions on the MetaD results.

The FES is expected to change with box dimension since both the intensity of the diffraction peaks used as CV and the melting temperature varies, as shown in Figures S6 and S7 of ESI.[23] Figure S6 shows the XRD patterns obtained by averaging the MD-NPT simulations for 2 ns at 2000 K for the simulation boxes containing 192, 648, 1536, 5182, 12288 and 24000 atoms. The main peaks shift toward lower angle and augment their intensity with an increase of the box size. The peak associated to the (111) plane (the one used to bias the simulations) does not vary for systems containing more than 5000 atoms, whereas the other two peaks reach convergence with the larger boxes.

Figure S7 shows that the melting temperature (determined using the two-phase coexistence method,[49] as proposed by Dozhdikov et al.[50] and described in the ESI) also varies with the simulation box dimension. T_m decreases as the system size increases, until it reaches convergence at around 2670 K. According to this result, it is expected that the FESs might be dependent on the simulation size if the same temperature is assumed. It is thus important to determine the computational melting temperature with the simulation size according to the force field to define the choice of the temperature in the MetaD simulations.

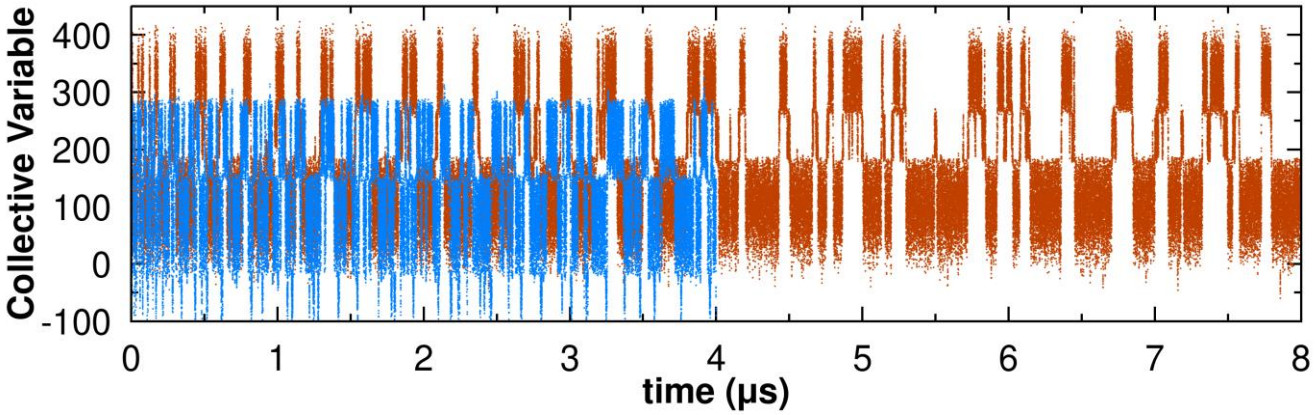

FIG. 14. Time evolution of the collective variable during 4 and 8 μs of metadynamics simulation of experiment n° 4 (ω=60, γ=50, σ=2) at 3200K using box containing respectively 192 (blue dots) and 648 atoms (orange dots)

Figure 14 compares the time evolutions of the biasing CV for MetaD simulations conducted at 3200 K using the parameters set of n° 4 (ω=60, γ=50, σ=2) on the systems with 192 and 648 atoms. It is clear that the transition frequency decreases with increasing box size. This is because the increase of the number of atoms augments the accessible configurational space, and, therefore, the complete crystallization of the entire simulation box becomes more difficult. Consequently, longer simulation time (4 μs) is required at the same temperature to obtain the converged FESs with 648 atoms with respect to the system with 192 atoms (1-2 μs).

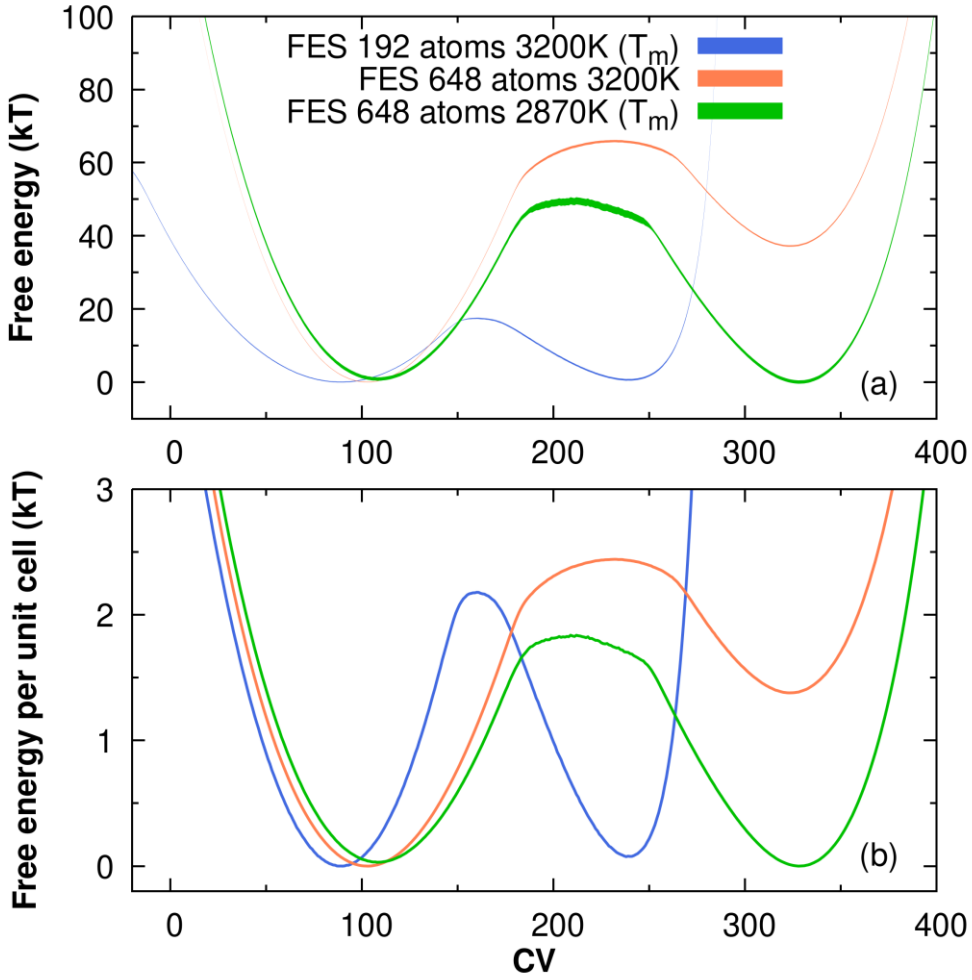

FIG. 15. (a) Comparison between FES at 3200K and at the respective melting temperatures of boxes containing 192 (3200 K) and 648 (2870 K) atoms; (b) FESs normalized by the unit cell number.

Figures 15 (a) shows the two FESs computed at 3200 K and at the respective melting temperatures of the 192 (3200 K) and 648 atomic (2870 K) systems. As expected, the energy barrier for crystallization increases with box dimension from 17 to 66 kT. This implies that different bias factor should be used depending on the simulation size. In the previous sections, we showed that the bias factor of 50 kT was optimal for the MetaD simulations with 192 atoms at 2700 K, but not at 3200 K. Indeed, the simulations at 3200 K converged faster (1 μs) with the lower bias factor (simulation n° 7, ω=60, γ=20, σ=2). The bias factor of 50 kT seems to be the best choice for the system with 648 atoms at 3200 K. Contrarily, at lower temperature, T_m=2870 K, this value is not optimal since the frequency of the transition jumps becomes too low to reach convergence. To accelerate the exploration of the phase space, we had to increase γ to 150.

The normalization of the FESs with respect to the number of the SiO_2 unit cells (figure 15 (b)) produces curves with comparable energy barrier, which allows us to make a rough estimation of the barrier height of the bigger system. Assuming the activation energy of ~2 kT per unit cell, we predict a barrier of 130 kT for the system containing 1536 atoms. Indeed, for the larger system, a bias factor of at least 150 or more was used to obtain enough number of crystallization events, as seen in Figure 16.

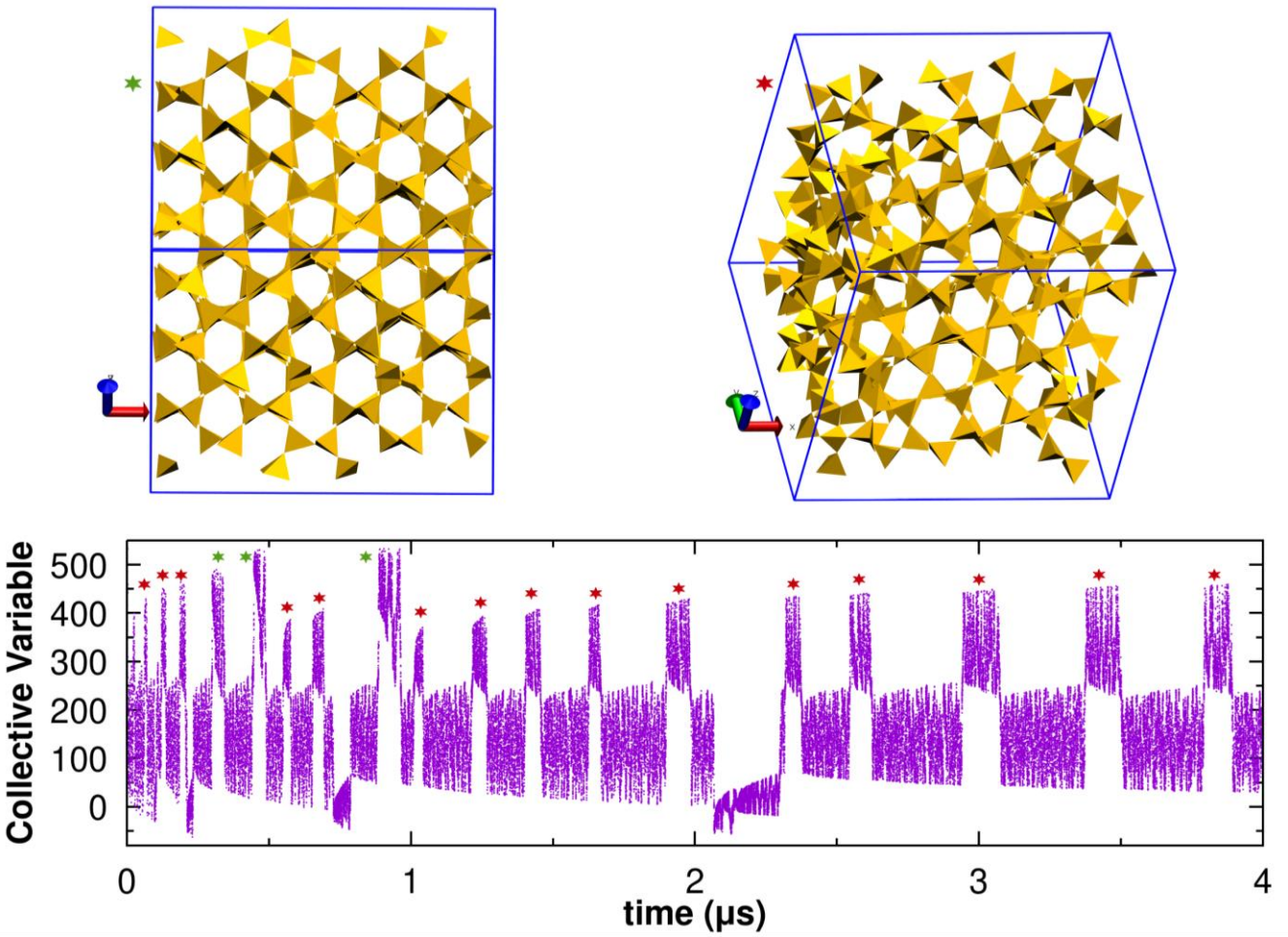

FIG. 16. Time evolution of the CV during the WTMetaD simulation with parameters ω=60, γ=250, σ=2 at 3200 K with the system containing 1536 atoms.

Despite a sufficient re-crossing frequency, most of the jumps (red asterisks in Figure 16) corresponds to incomplete crystallization. In fact, the perfect crystal is obtained only when the CV value reaches 400 units (green asterisks in Figure 16). Therefore, higher bias factor and longer simulation times are necessary to reach converged FES for the larger systems. For instance, the MetaD simulations of 4 μs for a system of 1536 atoms took 27 days on an Intel Xeon 6230 processor (2.10 GHz) with 20 cores. Such a substantial computational cost limits both system size and simulation time.

Although it is difficult to evaluate the converged FES including the complete crystallization path for the larger simulation systems, it is possible to understand the variations of the free energy with the crystal

nucleation of n atoms ($F(n)$) owing to the sufficient sampling of various configurations. To determine $F(n)$ the sampled configurations have been reweighted along the cluster dimension n using the same procedure proposed by Niu et al.[33] The local entropy fingerprint was used to identify crystal-like silicon atoms in the structure (see ESI for its definition).[51] We computed the adjacency matrix among those crystal-like atoms, and then the depth first search algorithm[52] was used to identify clusters and count the number of silicon atoms in them. As shown in Figure 17, FESs were evaluated as a function of n atoms. The free energies (at two temperatures, 3200 K and 2870 K) for the systems with 648 and 1536 atoms were calculated up to a critical value of n (n_c), which corresponds to the largest cluster size to avoid self-interaction of the nucleus (113 and 268 atoms, respectively).

The free energy curves at the same temperature are almost the same until 55 and 75 Si atoms at 2870 and 3200 K, respectively, implying that the initial formation of the crystalline nucleus is independent on the system size. After that, the crystal sizes varied in different ways: the crystal structures appeared in larger system steadily keep increasing, while those in the smaller systems plateau and then decrease. This is clearly a system size effect. $F(n)$ of the small system reaches a maximum and then decreases, as expected from CNT, but the critical nucleus is found to depend on the system size.

In CNT, the free energy is given by the formula:

$$\Delta F(n) = -\Delta\mu n + \sigma n^{2/3}$$

where $\Delta\mu$ is the chemical potential variation associated to melt-crystal phase transition, and σ is the interfacial energy. When cluster size is small enough, the free energy for nucleation should follow a 2/3 power low since the interfacial energy dominates. However, this is not true for our observations on the free energy curves at 2870 K up to n ~20 Si atoms. At the very beginning of the nucleation where n is less than 20, the free energy variation does not seem to follow the CNT prediction. Subsequently, at n > 20, the slope of the free energy curve increases more quickly up to n = 55-60 Si atoms. Figure 17 (a) shows that a few 6-membered rings form the initial embryo, whereas the larger clusters shown in Figure 17 (b) and (c) are made up by 6-membered rings interconnected to form the β-cristobalite crystal.

Therefore, it seems that the energy required to form crystalline nuclei whose size is larger than a critical size is not dominated by the formation of the 6-membered rings (which were indeed observed in the melt and in the glass structure)[53,54] but by the interconnection of these rings and their rearrangement along the right directions to form the perfect crystalline structure. Note that the initial slope of $F(n)$ at small n values is steeper at 3200 K compared to 2870 K, implying that even the formation of embryos is more difficult at higher temperature.

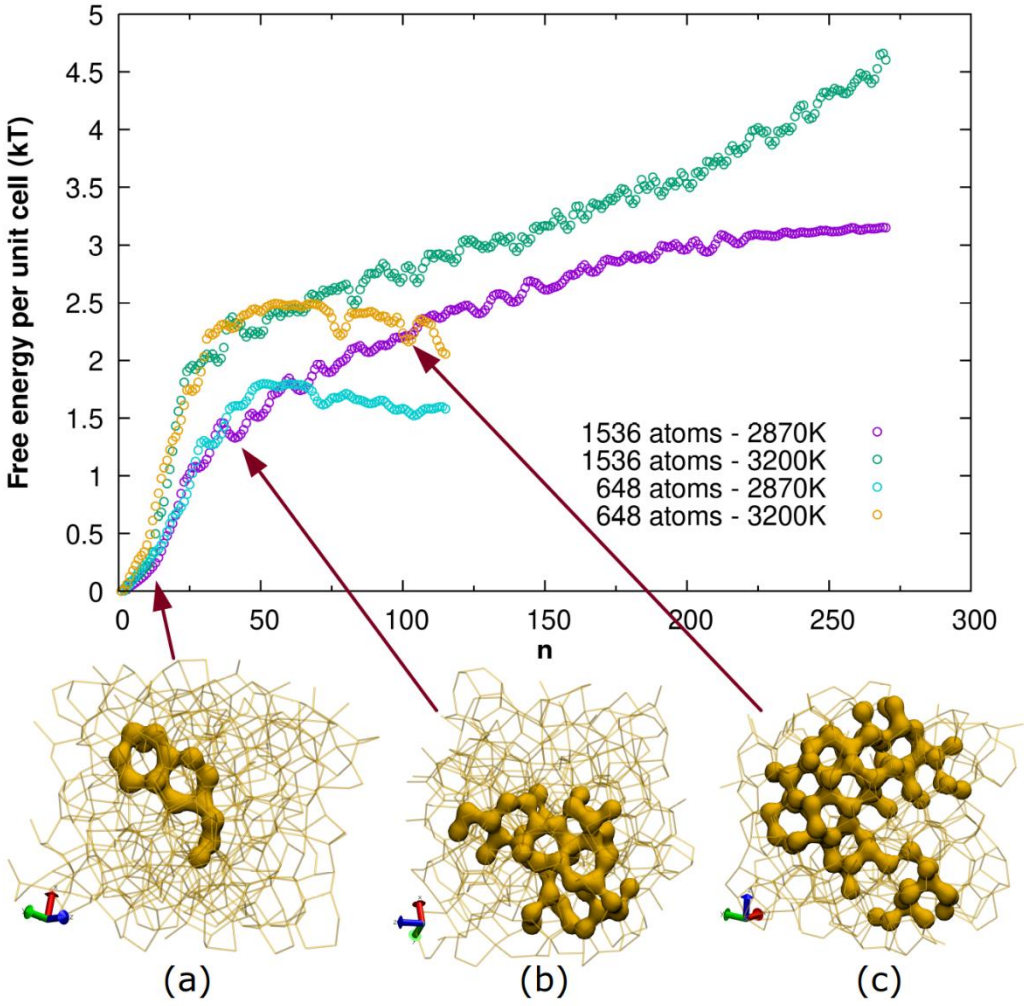

FIG. 17. Reweighted free energy per unit cell as a function of cluster size in term of n° of silicon atoms. The free energies at 3200 and 2870 K computed using the systems with 648 (216 Si atoms) and 1536 (512 Si atoms) atoms are compared. Snapshots (a)-(c) show structures containing a cluster with 15, 42 and 108 Si atoms. In these figures, only Si atoms are shown to highlight the order inside the structures.

V. CONCLUSIONS

In this work, we systematically investigated the effects of the simulation conditions to efficiently study thermodynamics of silica crystallization into β-cristobalite using MetaD simulations. First, we investigated the influence of the height (ω), width (σ) and bias factor (γ) used to define the biasing Gaussian potential. After that, the effects of the simulation temperature and system size were examined. Here is a summary of the results:

- Among the Metadynamics parameters (ω, σ and γ) the height value has only a minor effect on the final FES and the time to reach converged results. The width, σ, is effective to obtain converged FES. The appropriate value of σ depends on the fluctuation amplitude of the CV during conventional MD simulations: a half or a third of the fluctuation is a good choice. Too low or too large σ values prevent the convergence. The bias factor γ is the most important parameter; it substantially affects the time to reach convergence. A higher bias factor gives a higher re-crossing frequency, but it leads to deposit a large amount of bias and then explore high energetic configurations, which do not take part of the transformation. On the other hand, too low values require long simulation to reach the quasi-static regime. This parameter should be chosen in the same magnitude as the crystallization barrier. Unfortunately, this is not known a priori, and, thus, its estimation is the most difficult step. However, since this is proportional to the number of particles in the simulations one should roughly determine it by exploiting small simulation boxes.
- Temperature is another important parameter to study crystallization within a reasonable computational time. At $T > T_m$ the high mobility of the ions allows the fast exploration of the FES, which provides frequent observations of phase transitions. This allows convergence to be reached in significantly shorter time. Consequently, by increasing the temperature the optimal bias factor decreases. We also demonstrated that for high viscous systems such as silica the reliable FES at or below T_m can be estimated through temperature rescaling procedures.

- Size effects were observed for XRD patterns and melting temperature. Consequently, the FES depends on the simulation system size. However, the main characteristics of the FES representing the mechanism of crystallization are maintained.
- Large enough model would be necessary to observe the crystal growth until a real critical size, but the computational cost is too expensive. Even if the FES is not converged, the MetaD simulations provide useful information to understand the mechanism of crystal formation. To do so, a larger bias factor is efficient for the larger simulation models. The lower bound of the bias factor can be estimated from the barrier height for crystallization using smaller systems.
- By analyzing the free energy for nucleation of crystalline clusters as a function of their size, we found that the 6-membered rings form the initial embryos of nucleation. The energy penalty for the cluster formation steeply increases with an increase of the cluster size. The growth of the initial embryos is followed by structural rearrangements to build up the ideal crystalline structure.

ACKNOWLEDGMENTS

The work was supported by AGC Inc

DATA AVAILABILITY STATEMENT

The data that support the findings of this study are available from the corresponding author upon reasonable request.

REFERENCES

[1] W. Beckmann, *Crystallization: Basic Concepts and Industrial Applications* (John Wiley & Sons, 2013).

[2] W.A. Tiller, *The Science of Crystallization: Microscopic Interfacial Phenomena* (Cambridge University Press, Cambridge, 1991).

[3] C. Lin, C. Rüssel, and S. Dai, Prog. Mater. Sci. **93**, 1 (2018).

[4] H. Pan, S. Jiang, T. Zhang, and R. Tang, in *Methods Enzymol.*, edited by J.J. De Yoreo (Academic Press, 2013), pp. 129–144.

[5] V.M. Fokin, E.D. Zanotto, N.S. Yuritsyn, and J.W.P. Schmelzer, J. Non-Cryst. Solids **352**, 2681 (2006).

[6] W.J.E.M. Habraken, J. Tao, L.J. Brylka, H. Friedrich, L. Bertinetti, A.S. Schenk, A. Verch, V. Dmitrovic, P.H.H. Bomans, P.M. Frederik, J. Laven, P. van der Schoot, B. Aichmayer, G. de With, J.J. DeYoreo, and N.A.J.M. Sommerdijk, Nat. Commun. **4**, 1507 (2013).

[7] V.G. Baidakov and K.R. Protsenko, J. Phys. Chem. B **123**, 8103 (2019).

[8] S.C.C. Prado, J.P. Rino, and E.D. Zanotto, Comput. Mater. Sci. **161**, 99 (2019).

[9] A.O. Tipeev and E.D. Zanotto, Chem. Phys. Lett. **735**, 136749 (2019).

[10] A.O. Tipeev, E.D. Zanotto, and J.P. Rino, J. Phys. Chem. B **124**, 7979 (2020).

[11] J.R. Espinosa, C. Vega, C. Valeriani, and E. Sanz, J. Chem. Phys. **144**, 034501 (2016).

[12] L. Separdar, J.P. Rino, and E.D. Zanotto, Comput. Mater. Sci. **187**, 110124 (2021).

[13] Y. Sun, H. Song, F. Zhang, L. Yang, Z. Ye, M.I. Mendelev, C.-Z. Wang, and K.-M. Ho, Phys. Rev. Lett. **120**, 085703 (2018).

[14] A. Goswami, I.S. Dalal, and J.K. Singh, J. Chem. Phys. **153**, 094502 (2020).

[15] N.E.R. Zimmermann, B. Vorselaars, D. Quigley, and B. Peters, J. Am. Chem. Soc. **137**, 13352 (2015).

[16] F. Giberti, M. Salvalaglio, M. Mazzotti, and M. Parrinello, Chem. Eng. Sci. **121**, 51 (2015).

[17] E. Gaines, K. Maisuria, and D.D. Tommaso, CrystEngComm **18**, 2937 (2016).

[18] D. Quigley and P.M. Rodger, J. Chem. Phys. **128**, 221101 (2008).

[19] P.M. Piaggi, O. Valsson, and M. Parrinello, Phys. Rev. Lett. **119**, 015701 (2017).

[20] P. Ahlawat, A. Hinderhofer, E.A. Alharbi, H. Lu, A. Ummadisingu, H. Niu, M. Invernizzi, S.M. Zakeeruddin, M.I. Dar, F. Schreiber, A. Hagfeldt, M. Grätzel, U. Rothlisberger, and M. Parrinello, Sci. Adv. **7**, eabe3326 (n.d.).

[21] I. Ronneberger, W. Zhang, H. Eshet, and R. Mazzarello, Adv. Funct. Mater. **25**, 6407 (2015).

[22] P. Ahlawat, M.I. Dar, P. Piaggi, M. Grätzel, M. Parrinello, and U. Rothlisberger, Chem. Mater. **32**, 529 (2020).

[23] F. Lodesani, F. Tavanti, M.C. Menziani, K. Maeda, Y. Takato, S. Urata, and A. Pedone, Phys. Rev. Mater. **5**, 075602 (2021).

[24] G. Bussi and D. Branduardi, *Free-Energy Calculations with Metadynamics: Theory and Practice* (2015).

[25] Y.-Y. Zhang, H. Niu, G. Piccini, D. Mendels, and M. Parrinello, J. Chem. Phys. **150**, 094509 (2019).

[26] A. Laio and F.L. Gervasio, Rep. Prog. Phys. **71**, 126601 (2008).

[27] A. Barducci, G. Bussi, and M. Parrinello, Phys. Rev. Lett. **100**, 020603 (2008).

[28] P. Tiwary and M. Parrinello, J. Phys. Chem. B **119**, 736 (2015).

[29] T.M. Schäfer and G. Settanni, J. Chem. Theory Comput. **16**, 2042 (2020).

[30] O. Valsson, P. Tiwary, and M. Parrinello, Annu. Rev. Phys. Chem. **67**, 159 (2016).

[31] G. Bussi and G.A. Tribello, Methods Mol. Biol. (2019).

[32] B.E. Warren, *X-Ray Diffraction* (Courier Corporation, 1990).

[33] H. Niu, P.M. Piaggi, M. Invernizzi, and M. Parrinello, Proc. Natl. Acad. Sci. **115**, 5348 (2018).

[34] T. Karmakar, P.M. Piaggi, and M. Parrinello, J. Chem. Theory Comput. **15**, 6923 (2019).

[35] D. Quigley and P.M. Rodger, J. Chem. Phys. **128**, 154518 (2008).

[36] D.B. Peacor, Z. Für Krist. - Cryst. Mater. **138**, 274 (1973).

[37] A. Pedone, G. Malavasi, M.C. Menziani, A.N. Cormack, and U. Segre, J. Phys. Chem. B **110**, 11780 (2006).

[38] C.J. Fennell and J.D. Gezelter, J. Chem. Phys. **124**, 234104 (2006).

[39] S. Plimpton, J. Comput. Phys. **117**, 1 (1995).

[40] The PLUMED consortium, Nat. Methods **16**, 670 (2019).

[41] D.J. Evans and B.L. Holian, J. Chem. Phys. **83**, 4069 (1985).

[42] M.P. Allen and D.J. Tildesley, *Computer Simulation of Liquids* (Clarendon Press, 1989).

[43] G. Bussi and A. Laio, Nat. Rev. Phys. **2**, 200 (2020).

[44] G. Bussi, A. Laio, and P. Tiwary, in *Handb. Mater. Model. Methods Theory Model.*, edited by W. Andreoni and S. Yip (Springer International Publishing, Cham, 2020), pp. 565–595.

[45] M. Invernizzi and M. Parrinello, J. Chem. Theory Comput. **15**, 2187 (2019).

[46] Y. Crespo, F. Marinelli, F. Pietrucci, and A. Laio, Phys. Rev. E **81**, 055701 (2010).

[47] G. Bussi, F.L. Gervasio, A. Laio, and M. Parrinello, J. Am. Chem. Soc. **128**, 13435 (2006).

[48] G.A. Sycheva, Inorg. Mater. **56**, 1338 (2020).

[49] Y. Zou, S. Xiang, and C. Dai, Comput. Mater. Sci. **171**, 109156 (2020).

[50] V.S. Dozhdikov, A.Yu. Basharin, and P.R. Levashov, J. Chem. Phys. **137**, 054502 (2012).

[51] P.M. Piaggi and M. Parrinello, J. Chem. Phys. **147**, 114112 (2017).

[52] G.A. Tribello, F. Giberti, G.C. Sosso, M. Salvalaglio, and M. Parrinello, J. Chem. Theory Comput. **13**, 1317 (2017).

[53] B. Deng, Y. Shi, and F. Yuan, Materialia **12**, 100752 (2020).

[54] K. Vollmayr, W. Kob, and K. Binder, Phys. Rev. B **54**, 15808 (1996).